mm-Wave Complex Permittivity Extraction of LTCC Substrate Under the Influence of Surface Roughness

Ziad Hatab, *Student Member, IEEE*, Michael Gadringer, *Senior Member, IEEE*, Mariam Habib, and Wolfgang Bösch, *Fellow, IEEE*

***Abstract*— As many emerging technologies require the use of high-speed signals, the understanding of dielectric properties of materials used in manufacturing printed circuit boards (PCBs) is an essential aspect for accurate high-speed circuit designs, especially at millimeter-wave (mm-wave) frequencies. This work demonstrates a methodology for extracting complex relative permittivity of dielectric substrates covering mm-wave frequencies. For this purpose, low-temperature cofired ceramic (LTCC) substrate was measured up to 85 GHz and its complex relative permittivity was extracted. The approach used in this work is based on multiline thru–reflect–line (TRL) calibration for measuring the propagation constant and electromagnetic (EM) simulations to estimate the losses contributed by the conductor while accounting for surface roughness. An estimate of complex relative effective permittivity is obtained, from which the actual relative dielectric constant and the loss tangent of LTCC substrate are extracted. The estimated values for the relative dielectric constant and the loss tangent show an excellent agreement compared with the results obtained via split cavity resonator measurements.**

***Index Terms*— Electromagnetic (EM) simulation, low-temperature cofired ceramic (LTCC), permittivity, roughness, transmission line.**

I. Introduction

With the increasing usage of higher frequencies in modern communication systems, it becomes necessary to have broadband measurements of complex relative permittivity of dielectric substrates used to manufacture printed circuit boards (PCBs). Though there are industry standards on measuring the permittivity of substrates [1], [2], none of them is ideal for wideband measurements covering the millimeter-wave (mm-wave) frequency regime [3].

There are several methods to measure permittivity at high frequencies. Most of the methods are usually based on measuring a material sample directly via guided wave measurements [4]. These methods can be generalized into two categories: resonant method [5], [6] and transmission/reflection method [7], [8]. In the resonant method, permittivity is estimated from the *S*-parameters at resonance frequencies. As a result, the resonant methods can only provide permittivity measurements at sparse frequencies. It is, however, considered very accurate for the measurement of low-loss materials [6]. On the other hand, the transmission/reflection method is based on placing a sample between two waveguides, where the permittivity of the sample is estimated from the measured transmission and reflection coefficients. This approach can be applied in various ways: free-space [9], rectangular waveguide [8], and coaxial line [7]. The free-space method has the advantage of not requiring the sample to have the same cross section shape as the waveguide or coaxial line. However, the sample does require to be flat and sufficiently large. In this way, the impact of diffraction effects at the edges of the sample is minimized.

Apart from that, the transmission/reflection method demonstrated in [10] uses a guided Gaussian beam, which can be thought of as a hybrid between free-space and waveguide methods. This approach can ease the restriction on the shape and size of the sample. Generally, the transmission/reflection method is considered broadband. However, the frequency range it can cover is limited by the waveguide/fixture structures used in the setup. For example, the method demonstrated in [10] can generally cover frequencies in hundreds of gigahertz range. However, these measurements must be done in a frequency banded way. For example, the WR-12 waveguide can only be used for frequencies in the range of 55–90 GHz. Cascading measurements from different waveguides can introduce inconsistencies in the measurements across the frequency if the waveguides and fixtures are not machined with the same accuracy.

Many authors forget to mention one drawback when presenting waveguide methods for PCB substrate measurements: these measurements are of the substrate before metallization layer is applied on it. That is, the metallization process could affect the dielectric properties of the substrate, especially if chemical processes are involved.

A promising method to measure the permittivity of a substrate is based on planar transmission lines, which are manufactured on the measured substrate through a metallization process. For example, the differential phase length method [3] or the multiline thru–reflect–line (mTRL) calibration [11], [12] is used for such characterization purposes. They estimate the

Manuscript received September 13, 2021; revised December 26, 2021; accepted January 22, 2022. Date of publication February 16, 2022; date of current version March 11, 2022. This work was supported by the Austrian Federal Ministry for Digital and Economic Affairs and by the National Foundation for Research, Technology and Development. The Associate Editor coordinating the review process was Dr. Kamel Haddadi. *(Corresponding author: Ziad Hatab.)*

Ziad Hatab and Wolfgang Bösch are with the Institute of Microwave and Photonic Engineering, Graz University of Technology, 8010 Graz, Austria, and also with the Christian Doppler Laboratory for Technology Guided Electronic Component Design and Characterization (TONI), TU Graz, 8010 Graz, Austria (e-mail: z.hatab@tugraz.at; zi.hatab@gmail.com).

Michael Gadringer and Mariam Habib are with the Institute of Microwave and Photonic Engineering, Graz University of Technology, 8010 Graz, Austria.

Digital Object Identifier 10.1109/TIM.2022.3152319

propagation constant γ which describes the losses and the phase velocity of the wave traveling along the line. The planar transmission line methods have the advantage of providing broadband measurements covering frequencies from megahertz up to terahertz, possibly in one frequency sweep, as most planar transmission lines operate in the quasi-TEM mode. In addition, since these lines are manufactured on the same substrate, they share the same manufacturing tolerances.

The challenge in the planar transmission line method is the inability to obtain an accurate estimate of the characteristic impedance Z_0 of the line. This parameter, in addition to γ, is needed to describe a transmission line fully. By knowing both γ and Z_0, we can obtain the fundamental per-unit-length circuit parameters resistance (R), inductance (L), conductance (G), capacitance (C) (RLGC) of the line, by which we can achieve a separation between the conductor and dielectric loss

$$\gamma^2 = (R + j\omega L)(G + j\omega C) \tag{1}$$

$$Z_0^2 = (R + j\omega L)/(G + j\omega C). \tag{2}$$

The per-unit-length RLGC parameters presented in (1) and (2) relate directly to the material properties of a transmission line. They are assumed to be frequency-dependent. The resistance R and inductance L describe the conductor, while the conductance G and capacitance C are associated with the properties of the dielectric material. Therefore, by knowing these parameters, one can separate the influence of the conductor from the dielectric substrate. Thus, we can map C to the relative dielectric constant ϵ_r' and G to the loss tangent $\tan\delta$ of the substrate.

Given that γ is estimated by mTRL calibration, Z_0 remains to be determined. There are several methods to estimate Z_0, e.g., [13], [14]. However, these methods demand specific requirements for their applicability. For example, [13] can only be applied to transmission lines with lengths smaller than a quarter-wavelength of the maximum frequency. In addition, probing fixtures used to measure the line will significantly influence the measurement by imposing short transmission lines. Thus, such measurement conditions could falsify the results. Another method to estimate Z_0 is the calibration comparison method presented in [14]. This method can give an accurate estimate of Z_0 even with high shunt fixture capacitance and conductance. However, it fails when the fixtures are inductive. Unfortunately, this is almost always the case in PCB designs. Therefore, the calibration comparison method in [14] is only practical for miniature structures, e.g., semiconductor designs.

An alternative approach to estimate Z_0 is by calculating it from γ. If either $R + j\omega L$ or $G + j\omega C$ is known, Z_0 can be derived by

$$Z_0 = \frac{R + j\omega L}{\gamma} = \frac{\gamma}{G + j\omega C}. \tag{3}$$

In many works, e.g., [15], [16], they assume that the loss tangent $\tan\delta$ of the dielectric is very low, thus allowing them to neglect the term $G/(\omega C)$. In addition, they would assume that the distributed capacitance C is frequency-independent, thus measuring its value in the quasi-static sense [17]. These assumptions are generally valid if we discuss near-lossless materials and TEM propagation. However, such assumptions are usually not applicable in lossy materials and non-TEM transmission lines. For example, in the case of microstrip lines, the propagation mode is quasi-TEM, forcing the capacitance C to change with frequency. This behavior is observed due to the change in the E-field distribution with the increase in frequency.

We should also mention that other methods to characterize a dielectric substrate are based on model optimization, e.g., [18]. In such cases, the objective is to fit the frequency-dependent RLGC model to S-parameter measurements. However, such approaches are limited in applications to the low mm-wave regime. Such methods require that the model captures the waves' dynamics over the full investigated spectrum. However, this is not simple to come by, as not all planar transmission lines behave similarly and obey the generic frequency-dependent RLGC models. Even worse, the observed transmission line behavior gets more complex the higher the frequency gets.

The conductor surface roughness adds another layer of complexity. The added losses due to conductor roughness are most prominent when skin depth is in the range of roughness depth. However, the impact of roughness is a reasonably well-studied topic, and many good models already exist. For example, the physical model by Huray *et al.* [19] and Bracken [20] showed to predict the additional losses at mm-wave frequencies with reasonable accuracy. In addition, the recent "gradient model" from [21], which is based on the concept of frequency-dependent effective conductivity, agrees well with measurements at mm-wave frequencies.

Our approach in this article starts by measuring several similar microstrip lines of different lengths and performing an mTRL calibration [11] to extract the propagation constant γ. After that, we simulate the term $R + j\omega L$ while accounting for roughness. However, the goal is not to estimate Z_0 from the simulated $R + j\omega L$, but to estimate the conductor dispersion factor $R/(\omega L)$. By knowing $R/(\omega L)$, it is possible to calculate the effective dielectric constant and loss tangent from the propagation constant, from which the actual parameters of the substrate can be derived. The reasoning and theory for this approach are explained in Section II.

After that, Section III addresses surface roughness influence and how to account for it. In Section IV, we explain the process of mapping complex effective permittivity to the actual complex permittivity of the substrate. Finally, Section V and VI present the conducted experiment and finish with a conclusion.

II. Extracting the Effective Material Properties

As mentioned in the introduction, the per-unit-length frequency-dependent RLGC parameters of a transmission line relate directly to the medium's properties, in which the wave propagates. With the help of mTRL calibration, we can estimate the propagation constant γ. However, we also require Z_0 to compute the RLGC parameters

$$R + j\omega L = \gamma Z_0 \tag{4}$$

$$G + j\omega C = \gamma / Z_0. \tag{5}$$

To extract the complex permittivity of a dielectric substrate, we care primarily for C and G, as they relate directly to the dielectric properties. Therefore, if we perform an electromagnetic (EM) simulation to obtain an estimate of $R+j\omega L$, then it is possible to compute $G + j\omega C$ using γ obtained via mTRL calibration

$$G + j\omega C = \frac{\gamma_{\text{mTRL}}^2}{R_{\text{sim}} + j\omega L_{\text{sim}}}. \tag{6}$$

The reason that allows us to simulate R and L while not fully knowing ϵ_r' and $\tan\delta$ of the dielectric substrate is because of the weak dependency of L and R on ϵ_r' and $\tan\delta$ in a quasi-TEM propagation. We can further elaborate on this by writing the RLGC parameters in terms of field components, which were derived in [22] and [23] as

$$R = \frac{1}{|I(z)|^2}\iint \omega\mu''|\mathbf{H}_t(x,y,z)|^2 + \sigma|\mathbf{E}_l(x,y,z)|^2\,dxdy \tag{7}$$

$$L = \frac{1}{|I(z)|^2}\iint \mu'|\mathbf{H}_t(x,y,z)|^2 - \epsilon'|\mathbf{E}_l(x,y,z)|^2\,dxdy \tag{8}$$

$$G = \frac{1}{|V(z)|^2}\iint \sigma|\mathbf{E}_t(x,y,z)|^2 + \omega\mu''|\mathbf{H}_l(x,y,z)|^2\,dxdy \tag{9}$$

$$C = \frac{1}{|V(z)|^2}\iint \epsilon'|\mathbf{E}_t(x,y,z)|^2 - \mu'|\mathbf{H}_l(x,y,z)|^2\,dxdy \tag{10}$$

where

$$\mathbf{E}(x,y,z) = \mathbf{E}_t(x,y,z) + \mathbf{E}_l(x,y,z) \tag{11}$$

$$\mathbf{H}(x,y,z) = \mathbf{H}_t(x,y,z) + \mathbf{H}_l(x,y,z) \tag{12}$$

are the solutions to Maxwell's equations for the single-mode propagation. The subscripts "t" and "l" denote transversal (xy-plane) and longitudinal (z: propagation direction) components, respectively. The complex material properties ϵ and μ are defined as

$$\epsilon = \epsilon' - j\sigma/\omega \tag{13}$$

$$\mu = \mu' - j\mu'' \tag{14}$$

where the real parts describe the energy storage and the imaginary parts the losses. Both (13) and (14) are spatial-dependent in the transversal domain, i.e., xy-plane. Therefore, ϵ and μ describe both the dielectric and the conductor as a piecewise function. Furthermore, we assume an isotropic material, i.e., ϵ and μ are not tensor quantities.

Equations (7) and (8) are general descriptors for R and L for a single-mode propagation described by (11) and (12). However, for a broad class of applications, we can simplify the expressions in (7) and (8) by limiting our analysis to TEM propagation and nonmagnetic medium, i.e., $\mu' = \mu_0$ and $\mu'' = 0$. By TEM mode, we refer here to the lossy TEM mode. Under the assumption of TEM propagation, all external longitudinal components are zero, that is, $\mathbf{E}_l(x,y,z) = 0$ for any x, y points outside the conductor area. The only longitudinal components that remain are the ones inside the conductor due to its finite conductivity. Therefore, (7) and (8) simplify to

$$R = \frac{1}{|I(z)|^2}\iint_{\text{Conductor}} \sigma|\mathbf{E}_l(x,y,z)|^2\,dxdy \tag{15}$$

$$L = \frac{\mu_0}{|I(z)|^2}\iint |\mathbf{H}_t(x,y,z)|^2\,dxdy - \frac{1}{|I(z)|^2}\iint_{\text{Conductor}} \epsilon'|\mathbf{E}_l(x,y,z)|^2\,dxdy. \tag{16}$$

The only integral covering the external fields in the dielectric is the first term in (16). Yet, this integral does not depend on the dielectric properties of the substrate (assuming $\mu' = \mu_0$). In conclusion, both L and R are independent of the dielectric properties of the substrate for TEM propagation and nonmagnetic materials.

Although we showed that simulating R and L is a valid approach to obtain estimates for their values, the problem in trying to simulate R and L is the uniqueness of their values, as both the quantities depend on the z-component normalization, i.e., $I(z)$. The uniqueness issue stems from the definition of the characteristic impedance, which can be written in three ways [24]

$$\text{Power–Current} \quad Z_0 = P(z)/|I(z)|^2 \tag{17}$$

$$\text{Power–Voltage} \quad Z_0 = |V(z)|^2/P^*(z) \tag{18}$$

$$\text{Voltage–Current} \quad Z_0 = V(z)/I(z) \tag{19}$$

where $(\cdot)^*$ denotes the complex conjugate operator. For the discussion below, we drop the z dependency for notational simplicity. The uniqueness issue of Z_0 arises when $P \neq VI^*$, which leads to the three expressions for Z_0 not being equal. In fact, this is the case for non-TEM propagation. If we take a microstrip line as an example, which supports a quasi-TEM mode, the value of V is dependent on the choice of the integration line, over which the E-field is integrated. However, depending where this line is chosen, different values for V will be obtained, thus leading to different values for Z_0. Therefore, as a consequence, the values for R and L are also not unique. It should be noted that the propagation constant γ is unique for each propagation mode, even for non-TEM modes. The uniqueness issue appears only in the magnitude of Z_0.

The question on hand becomes: which definition of Z_0 is the correct one for a microstrip line? Brews investigated this question in [24], where he concluded that all the definitions of Z_0 become equal if $P = VI^*$ is enforced. However, Brews also concluded that even after imposing $P = VI^*$, the uniqueness issue of Z_0 does not disappear, because the magnitudes of I and V are still arbitrary and depend on their definition, but their relative phase remains unchanged.

Therefore, finding a unique Z_0 for a microstrip line should not be the objective. As a matter of fact, for the sole purposes of extracting the material properties of a dielectric substrate, we do not need to know Z_0 fully. We only need to know its phase. To elaborate on this, we rearrange (1) and (2) to equal

$$\gamma^2 = \omega^2 LC\left(\frac{R}{\omega L} + j\right)\left(\frac{G}{\omega C} + j\right) \tag{20}$$

$$Z_0^2 = \frac{L}{C}\left(\frac{R}{\omega L} + j\right)\Big/\left(\frac{G}{\omega C} + j\right). \tag{21}$$

The quantities $R/(\omega L)$ and $G/(\omega C)$ are the effective dispersion factors of the conductor and the dielectric substrate, respectively, and the term LC equals the effective dielectric constant. The interesting part about these quantities is that they are normalization-independent. That is, regardless how V and I are defined, $R/(\omega L)$, $G/(\omega C)$, and LC are unaffected [23]. However, the same does not apply to L/C. Nevertheless, for the sole purpose of extracting the complex permittivity of a substrate, we only need to know LC and $G/(\omega C)$, which map directly to ϵ_r' and $\tan\delta$, respectively. The mapping of these quantities is discussed in Section IV.

The values for $R/(\omega L)$, $G/(\omega C)$, and LC can be obtained in the following order.

1) Estimating $R/(\omega L)$ through EM simulation of the concerned transmission line. From the simulated Z_0 and γ, $R/(\omega L)$ is calculated as

$$\frac{R}{\omega L} = \frac{\mathcal{R}e\{\gamma_{\text{sim}} Z_{0,\text{sim}}\}}{\mathcal{I}m\{\gamma_{\text{sim}} Z_{0,\text{sim}}\}}. \tag{22}$$

2) After obtaining an estimate for $R/(\omega L)$ via (22), we determine $G/(\omega C)$ from mTRL measurements of γ via a reformulation of (20) to solve for $G/(\omega C)$

$$\frac{G}{\omega C} = \frac{M - R/(\omega L)}{MR/(\omega L) + 1} \tag{23}$$

where $M = -\mathcal{I}m\{\gamma_{\text{mTRL}}^2\}/\mathcal{R}e\{\gamma_{\text{mTRL}}^2\}$.

3) The final step is to compute LC. This factor can be derived by rearranging (20) to solve for LC

$$LC = \frac{|\gamma_{\text{mTRL}}^2|}{\omega^2\sqrt{\left(\left(\frac{R}{\omega L}\right)^2+1\right)\left(\left(\frac{G}{\omega C}\right)^2+1\right)}}. \tag{24}$$

III. Accounting for Surface Roughness

The impact of surface roughness on losses is most prominent when skin depth is in the range of roughness depth. Essentially, roughness causes an increase in losses due to the finite conductivity of a conductor. As a result, this makes the distinguish between dielectric and conductor losses more difficult. Generally, the losses of a conductor can be divided into two mechanisms: skin loss, which is proportional to $\sqrt{f}$, and roughness loss, which is proportional to f [21]. Considering these relationships, we can deduce the following observation.

1) Losses due to roughness start at frequencies at which skin depth is in the same range of rms roughness depth (commonly in the lower μm regime).
2) It is known that the dielectric loss due to polarization (i.e., loss tangent) increases with frequency (e.g., Djordjevic–Sarkar model [25]). At the lower end of the spectrum, transmission line losses are primarily due to the conductor. However, at higher end, both the dielectric and conductor contribute to the losses.

From the above observations, we can conclude that the effects of conductor roughness can be separated from the dielectric loss at lower frequencies, where skin depth approaches roughness depth. We can further analyze the impact of roughness quantitatively by referring to the empirical roughness model by Hammerstad and Jensen [26]

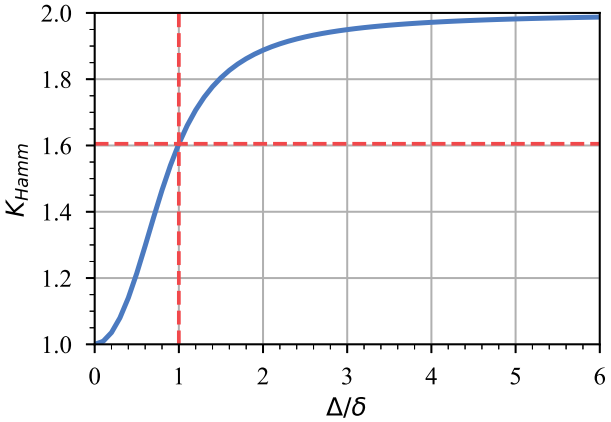

Fig. 1. Hammerstad roughness model as a function of the ratio of roughness depth to skin depth Δ/δ.

$$K_{\text{Hamm}} = \frac{\alpha_{\text{rough}}}{\alpha_{\text{smooth}}} = 1 + \frac{2}{\pi}\arctan\left(1.4\left(\frac{\Delta}{\delta(f)}\right)^2\right) \tag{25}$$

where α_{rough} and α_{smooth} are the losses per unit length of a transmission line with a rough and smooth conductor surface, respectively. Δ is the rms roughness depth, and $\delta(f) = 1/(\pi\sigma\mu f)^{1/2}$ is the skin depth.

A plot of (25) is shown in Fig. 1, where we can observe that the added loss due to roughness increases dramatically when roughness depth starts to approach skin depth. For example, when the skin depth equals roughness depth, i.e., $\Delta/\delta = 1$, the additional losses due to roughness reach 60%.

In the case of low-temperature cofired ceramic (LTCC) measurements presented in Section V, the copper roughness is estimated to be around 0.7 μm. Therefore, the added loss due to this roughness is expected to be notable between frequencies 4 and 8 GHz, where the skin depth is in the range of 1.2–0.72 μm. In addition, we also know from a separate measurement that the dielectric loss of LTCC is negligibly small in this frequency range, i.e., up to 8 GHz losses observed in measurements are primarily due to skin and roughness losses.

It should be noted that (25) is not entirely accurate at mm-wave frequencies. It saturates reasonably quickly and provides a maximum correction of 2, which has been shown in many publications to be not the case. In [27], a scaling factor was introduced to increase the limit beyond 2. Even with the inclusion of the correction factor, the Hammerstad model is fundamentally unable to accurately predict roughness loss at higher frequencies, as it was derived based on heuristic methods. Therefore, in this article, we use the causal Huray model [20], which is given by

$$K_{\text{CH}} = 1 + \frac{3}{2}\frac{N}{A_{\text{flat}}}\frac{4\pi a^2}{1 + \left(2j\left(\frac{a}{\delta(f)}\right)^2\right)^{-1/2}} \tag{26}$$

where N is the number of stacked snowballs (spheres) covering a flat area A_{flat}, and a is the radius of the snowball. As (26) is already implemented in the full-wave EM simulation

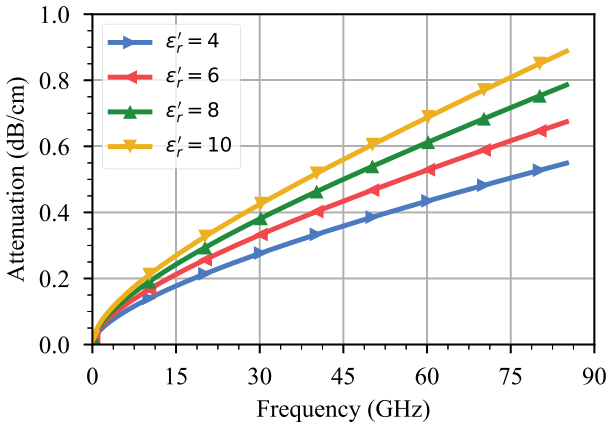

Fig. 2. Simulated attenuation per-unit-length of a microstrip line for a range of values of ϵ'_r, while maintaining $\tan\delta = 0$.

software Ansys high frequency structure simulator (HFSS), the goal is to fit the simulation data to the measurements at the low-frequency regime. At this regime, the losses due to roughness are present, while the losses due to dielectric substrate are negligible.

Since we can estimate the propagation constant γ via mTRL calibration, we have access to the total attenuation per unit length $\alpha = \mathcal{R}e\{\gamma\}$. One possible way to obtain the needed parameters in (26) is by fitting the simulated attenuation α_{Sim} to the attenuation from mTRL measurements α_{mTRL}. However, this approach can lead to inaccurate fitting because α depends as well on ϵ'_r, i.e., the dielectric constant of the substrate, which, at this point, is still unknown. To elaborate on this, we can express α as a function of RLGC parameters, which can be derived from (20) to give

$$\alpha^2 = \frac{\omega^2 LC}{2}\left[\frac{R}{\omega L}\frac{G}{\omega C} - 1 + \sqrt{\left(\frac{R^2}{\omega^2 L^2}+1\right)\left(\frac{G^2}{\omega^2 C^2}+1\right)}\right] \tag{27}$$

where the terms $R/(\omega L)$ and $G/(\omega C)$ are the effective dispersion factors of the conductor and the dielectric substrate, respectively. They describe the associated losses. The term LC is inversely proportional to the square of the speed of light in vacuum c_0. The proportionality factor is the relative effective dielectric constant $\epsilon'_{\text{r,eff}}$ if the material is nonmagnetic

$$LC = \mu'_{\text{eff}}\epsilon'_{\text{eff}} \xrightarrow{\mu'_{\text{eff}}=\mu_0} LC = \mu_0\epsilon_0\epsilon'_{\text{r,eff}} = \frac{\epsilon'_{\text{r,eff}}}{c_0^2}. \tag{28}$$

In conclusion, we can see from (27) and (28) that even if we assume that the dielectric material has zero losses, i.e., $G/(\omega C) = 0$, we still have the factor LC amplifying the conductor losses, as demonstrated in (27). Hence, LC introduces a dependency of the conductor losses on the dielectric constant. That is, the higher the dielectric constant, the higher the losses. It should be noted that when $R/(\omega L) = G/(\omega C) = 0$, then $\alpha = 0$. Thus, the dielectric constant only influences the losses when at least $R/(\omega L)$ or $G/(\omega C)$ is nonzero. The plot in Fig. 2 visualizes the influence of the substrate dielectric constant on α, even if the loss tangent of the substrate is zero.

Therefore, the use of α for estimating the model parameters of the roughness model is not practical due to the dependency on ϵ'_r. Instead, we define the ratio of the imaginary part γ^2 to its real part, which is given by

$$\frac{-\mathcal{I}m\{\gamma^2\}}{\mathcal{R}e\{\gamma^2\}} = \left(\frac{R}{\omega L}+\frac{G}{\omega C}\right)\Big/\left(1-\frac{R}{\omega L}\frac{G}{\omega C}\right). \tag{29}$$

The expression in (29) is only dependent on the loss terms, which is more suitable for finding the optimal parameters for the roughness model. Suppose $G/(\omega C) \approx 0$ in the frequency range between f_1 and f_2, we formulate the optimization problem to estimate the best parameters of the roughness model in (26) as

$$\underset{\substack{\sigma_{\text{dc}}\\ N/A_{\text{flat}}\\ a}}{\text{argmin}} \sum_{f=f_1}^{f_2}\left|\frac{-\mathcal{I}m\{\gamma^2_{\text{mTRL}}\}\omega}{\mathcal{R}e\{\gamma^2_{\text{mTRL}}\}c_0} - \frac{-\mathcal{I}m\{\gamma^2_{\text{Sim}}\}\omega}{\mathcal{R}e\{\gamma^2_{\text{Sim}}\}c_0}\right|^2. \tag{30}$$

The minimization problem in (30) is used to find the best parameters for the roughness model in (26), i.e., N/A_{flat} and a, while also estimating the dc conductivity σ_{dc} of the conductor. Generally, the inclusion of σ_{dc} in the optimization is not necessary, if σ_{dc} is already known via another measurement method. Furthermore, the objective function in (30) is scaled by ω/c_0 to eliminate frequency normalization and to scale up the values.

IV. Mapping Functions

The general way to map the quantities LC and $G/(\omega G)$ to ϵ'_r and $\tan\delta$ is to find mathematical models that relate these quantities to each other. One way is to use well-known formulas from the literature. For example, the relationship for $\epsilon'_{\text{r,eff}}$ of a microstrip line by Kirschning and Jansen (K&J) [28] has broad applicability and promises accuracy better than 0.6%. However, such models were derived for lossless transmission lines and were verified for limited frequency range. Generally, these models only provide an approximation and are meant to be used as synthesis equations for design purposes.

A more accurate way to obtain a mapping function is to generate a mathematical model for a specific geometry via EM simulations. The principle is to fit simulation data to a polynomial of Nth order. This gives the advantage to model arbitrary geometry, e.g., microstrip line, slotline, (grounded) coplanar waveguide, and stripline. In the below discussion, we simplify notation by defining

$$\epsilon'_{\text{r,eff}} = c_0^2 LC \tag{31}$$

$$\tan\delta_{\text{eff}} = G/(\omega C). \tag{32}$$

We begin the discussion by modeling $\epsilon'_{\text{r,eff}}$ as a polynomial of Nth order

$$\epsilon'_{\text{r,eff}} = \sum_{n=0}^{N}(\epsilon'_{\text{r}})^n a_n \tag{33}$$

where the coefficients a_n are frequency-dependent. To find the coefficients a_n, the simulation data for $\epsilon'_{\text{r,eff}}$ are generated for different values of ϵ'_{r}. After that, the coefficients are determined via least-squares solution at every frequency point. To illustrate this, we assume $N = 2$, and M simulation data

points were generated, where $M > N$. Then the corresponding equation system can be composed as

$$\underbrace{\begin{bmatrix} \epsilon'_{\mathrm{r,eff}}[1] \\ \epsilon'_{\mathrm{r,eff}}[2] \\ \vdots \\ \epsilon'_{\mathrm{r,eff}}[M] \end{bmatrix}}_{\mathbf{b}} = \underbrace{\begin{bmatrix} 1 & \epsilon'_{\mathrm{r}}[1] & (\epsilon'_{\mathrm{r}})^2[1] \\ 1 & \epsilon'_{\mathrm{r}}[2] & (\epsilon'_{\mathrm{r}})^2[2] \\ \vdots & \vdots & \vdots \\ 1 & \epsilon'_{\mathrm{r}}[M] & (\epsilon'_{\mathrm{r}})^2[M] \end{bmatrix}}_{\mathbf{A}} \underbrace{\begin{bmatrix} a_0 \\ a_1 \\ a_2 \end{bmatrix}}_{\mathbf{x}} \tag{34}$$

where $\epsilon'_{\mathrm{r}}[1] \leq \epsilon'_{\mathrm{r}} \leq \epsilon'_{\mathrm{r}}[M]$, that is, the model is valid within the simulated range of values for ϵ'_{r}. The solution for $\mathbf{x}$ is found by taking the pseudo-inverse of $\mathbf{A}$

$$\mathbf{x} = \left(\mathbf{A}^T\mathbf{A}\right)^{-1}\mathbf{A}^T\mathbf{b}. \tag{35}$$

After solving for the coefficient a_n, the relative dielectric constant ϵ'_{r} can be derived by solving the quadratic equation using the estimated $\epsilon'_{\mathrm{r,eff}}$ from mTRL measurements as detailed in Section II

$$\epsilon'_{\mathrm{r}} = \frac{2(a_0 - \epsilon'_{\mathrm{r,eff}})}{-a_1 - \sqrt{a_1^2 - 4a_2(a_0 - \epsilon'_{\mathrm{r,eff}})}}. \tag{36}$$

The solution in (36) is expressed using the alternative form of the standard quadratic formula [29]. This formula is robust against degenerate cases, e.g., if $a_2 = 0$, which means the model reduces to a linear order.

To illustrate the accuracy of the polynomial model for different orders, a microstrip line, as depicted in Fig. 3, is simulated for values of ϵ'_{r} in the range $\epsilon'_{\mathrm{r}} \in [4, 10]$. The coefficient a_n is extracted for the polynomial orders $N = \{1, 2, 3\}$. Then, the same microstrip line is simulated again while ϵ'_{r} is set to random values in the range $\epsilon'_{\mathrm{r}} \sim \mathcal{U}(4, 10)$ across the simulated frequencies. The simulation was done in Ansys HFSS, where only the wave ports were simulated, i.e., 2-D simulation. Since we only need Z_0 and γ from the simulation and not the S-parameters, it is sufficient to only simulate the wave ports. In addition, by only simulating the wave ports, we reduce the simulation time significantly as only 2-D meshes are considered. The definition of Z_0 chosen in this simulation example was the power current, as given by (17). However, other definitions of Z_0 could be used, as the quantities $G/(\omega C)$, $R/(\omega L)$, and LC are normalization-independent (see Section II).

Fig. 4 depicts the result of the model for different polynomial orders. In addition, the K&J model [28] is included for comparison. The figure shows that the K&J model has a higher error than the proposed polynomial approach. However, the result of the K&J model does agree with its claim of accuracy better than 0.6%. The first-order polynomial seems to behave similar to the K&J model at higher frequencies. In contrast, the second- and third-order seem to give the same results, which indicate that there is no need to increase the model order beyond the second-order in this example. It should also be noted that the required polynomial order depends on the range of ϵ'_{r} values being considered, as well as the geometry of the transmission line.

To demonstrate the invariability of $R/(\omega L)$ with respect to the change in the dielectric constant of the substrate, we plotted $R/(\omega L)$ in Fig. 5 using the same random ϵ'_r, as well as a constant $\epsilon'_r = 8$. We can see from Fig. 5 that even with abrupt change in ϵ'_r, negligible influence can be seen in $R/(\omega L)$.

Regarding loss tangent modeling, there is less work found in the literature. However, it is common to derive the loss

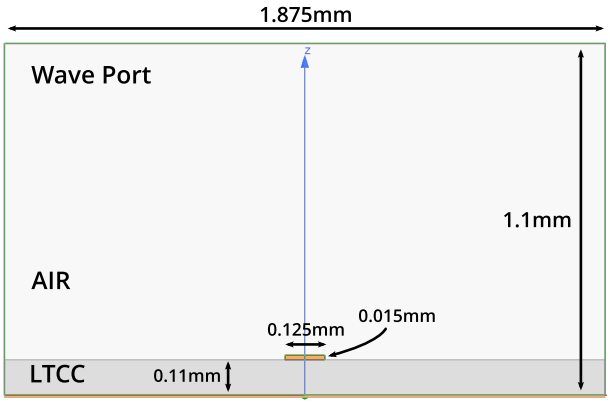

Fig. 3. Microstrip line simulated in Ansys HFSS. This is a 2-D simulation, where only the wave ports were simulated to extract Z_0 and γ of the microstrip line.

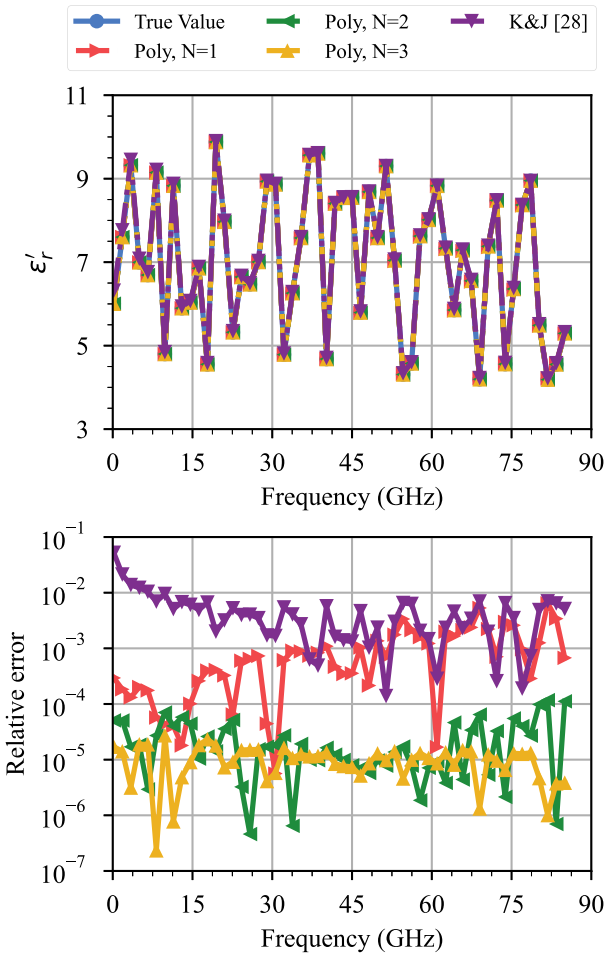

Fig. 4. Example of mapping $\epsilon'_{\mathrm{r,eff}}$ to ϵ'_{r} using the polynomial model with different orders and comparing it with the K&J model.

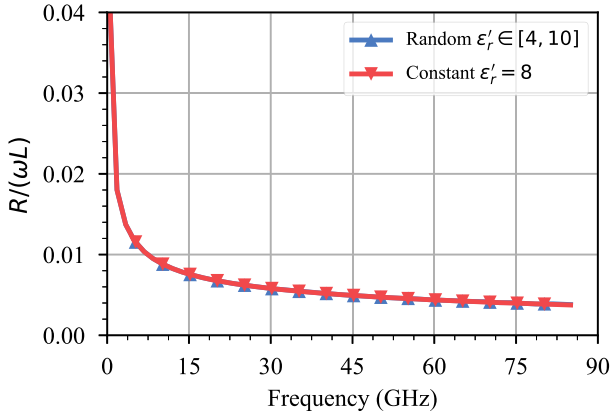

Fig. 5. Demonstrating the invariability of $R/(\omega L)$ with respect to the change in ϵ_r' of the substrate.

tangent using the models of effective dielectric constant. The concept follows the idea of expressing the complex relative effective permittivity as a weighted sum of the two dielectric materials as

$$\epsilon_{\mathrm{r,eff}} = \epsilon_{\mathrm{r}} q + (1-q)\epsilon_{\mathrm{r2}} \tag{37}$$

where $\epsilon_{\mathrm{r2}} = 1$ if the top dielectric is air, and q is called the filling factor, which describes the percentage of the field contained in the lower substrate. In many textbooks, the concept of the filling factor is discussed primarily in the context of development of analytical models for the static effective dielectric constant. In these cases, the parameter q is assumed to only depend on the transmission line's geometry [30]. However, if we already know $\epsilon_{\mathrm{r,eff}}'$ and ϵ_{r}', the filling factor q can be expressed as

$$q = \frac{\epsilon_{\mathrm{r,eff}}' - 1}{\epsilon_{\mathrm{r}}' - 1}. \tag{38}$$

Then, the loss tangent $\tan\delta$ is determined by inserting (38) in (37) and reformulating it in terms of $\tan\delta_{\mathrm{eff}}$, $\epsilon_{\mathrm{r,eff}}'$, and ϵ_{r}'

$$\tan\delta = \frac{\epsilon_{\mathrm{r,eff}}'}{\epsilon_{\mathrm{r}}' q}\tan\delta_{\mathrm{eff}} = \frac{\epsilon_{\mathrm{r,eff}}'}{\epsilon_{\mathrm{r}}'}\frac{\epsilon_{\mathrm{r}}' - 1}{\epsilon_{\mathrm{r,eff}}' - 1}\tan\delta_{\mathrm{eff}}. \tag{39}$$

We can also develop a model for $\tan\delta_{\mathrm{eff}}$ based on a polynomial approximation, similar to (33)

$$\tan\delta_{\mathrm{eff}} = \sum_{n=0}^{N} (\tan\delta)^n b_n \tag{40}$$

where b_n is dependent on both the frequency and ϵ_{r}. Therefore, when computing the coefficients b_n using least-squares solution, the simulation to generate values for $\tan\delta_{\mathrm{eff}}$ must be performed using ϵ_{r}' obtained from (36). That is, the process must be sequential; first estimate ϵ_{r}' and then $\tan\delta$. For the quadratic case, the solution for $\tan\delta$ is calculated similar to (36) as

$$\tan\delta = \frac{2(b_0 - \tan\delta_{\mathrm{eff}})}{-b_1 - \sqrt{{b_1}^2 - 4b_2(b_0 - \tan\delta_{\mathrm{eff}})}}. \tag{41}$$

Fig. 6 shows the results of simulating a microstrip line with random values of $\tan\delta$ across the frequency. This progression is approximated by the polynomial model with different orders

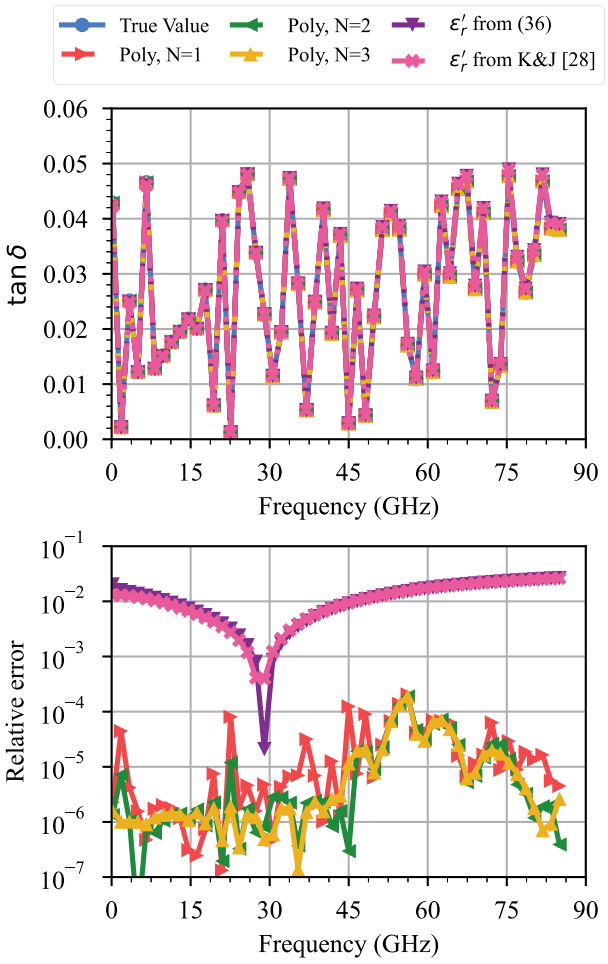

Fig. 6. Example of mapping $\tan\delta_{\mathrm{eff}}$ to $\tan\delta$ using the polynomial model with different orders and comparing it with (39).

and expression (39). For the latter case, ϵ_{r}' was computed from (36), or it was evaluated from the K&J model [28]. Interestingly, using (39) with ϵ_{r}' computed from the K&J model [28] shows a similar result to the case when ϵ_{r}' was computed by (36). However, the polynomial models outperform (39). Furthermore, it appears that a first-order model is sufficient to capture the values of $\tan\delta$ in this example.

The uncertainty propagation of the presented models can be accomplished following the guidelines in [31] and [32].

V. Experiment and Results

A. mTRL Calibration

The goal of performing an mTRL calibration is to estimate the propagation constant of the line standards used in calibration. Therefore, we only need the line standards for this purpose. The reflect standard is only necessary if the calibration coefficients are required as well. The error box model of mTRL is given by

$$\mathbf{M}_i = \mathbf{A}\begin{bmatrix} e^{-\gamma l_i} & 0 \\ 0 & e^{\gamma l_i} \end{bmatrix}\mathbf{B} \tag{42}$$

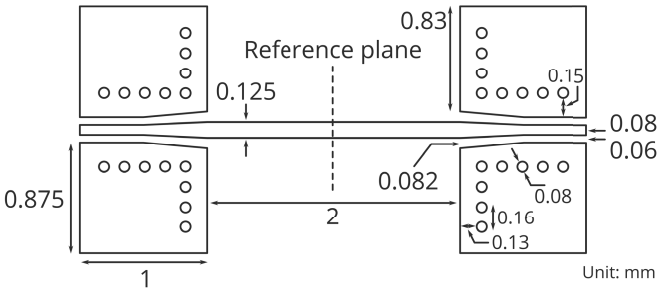

Fig. 7. Dimensions of the Thru standard of the mTRL kit (unit: mm). The reference plane is defined in the middle of the structure and all other lines are referenced to this plane.

where **A** and **B** are the left and right unknown error boxes, respectively (i.e., the calibration coefficients), l_i is the length of the ith line, and γ is the propagation constant. All the matrices are given in terms of cascade parameters (T-parameters). The principle of mTRL calibration is to form pairs of lines of different length, where one line is common among all the pairs. Finally, we form the following eigenvalue problem for each line pair:

$$\mathbf{M}_i\mathbf{M}_j^{-1} = \mathbf{A}\begin{bmatrix} e^{-\gamma(l_i-l_j)} & 0 \\ 0 & e^{\gamma(l_i-l_j)} \end{bmatrix}\mathbf{A}^{-1}. \tag{43}$$

After solving the eigenvalue problem above for the considered line pairs, the final result for the propagation constant is derived through a weighted sum based on the Gauss–Markov method [11], [12]. It should be noted that for the error box model given in (42) and (43), we assume that the isolation terms of the vector network analyzer (VNA) are negligible, which is generally true in modern VNAs. Also, we assume that the switch terms were already accounted for, which can be directly measured from a four-receiver VNA.

The experiment we conducted consists of measuring multiple microstrip lines with different lengths fabricated on an LTCC substrate using the fixture structure depicted in Fig. 7. The fabricated microstrip lines were designed to have 50 Ω characteristic impedance, which resulted in a strip width of 125 ± 3 μm and a thickness of 15 ± 5 μm. The LTCC substrate was 110 μm thick with $\epsilon_r' = 7.9$ and $\tan\delta = 0.0015$ at 79 GHz. These values were obtained from a separate split cavity resonator measurement for a different substrate thickness and before metallization was applied.

The experiment we conducted was done on a probe station using 150 μm pitch ground-signal-ground (GSG) RF probes connected to a VNA. Since we are working with GSG probes, the microstrip lines were tapered to a grounded coplanar waveguide interface. The dimensions of the Thru standard are shown in Fig. 7. The length of the lines is referenced to the middle of the Thru standard, i.e., the reference plane indicates the line length of zero.

The lengths of the microstrip lines we considered are {0, 0.35, 1.5, 7, 31} mm. The measurement was conducted in the frequency range of 0.2–85 GHz. We first performed an line-reflect-reflect-match (LRRM) calibration on an impedance standard substrate (ISS) to shift the reference plane to the tips of the probes. The LRRM calibration process is automated by our semiautomated probe station. The initial LRRM calibration is generally not required, but as the probes themselves were manually controlled (the chuck is automated), we had to realign them manually every time we measured a new line standard. Therefore, having the reference plane at the probe's tips helps us align the probes accurately. In Fig. 8, we show the corresponding measurement setup.

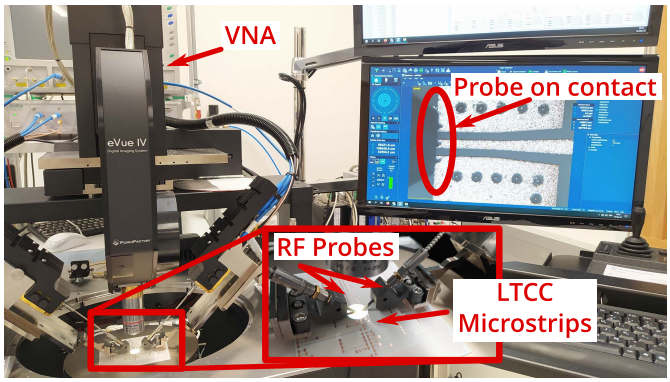

Fig. 8. Experiment hardware: probe station, VNA, RF probes, and LTCC microstrip lines.

B. Parameters Extraction

In the first step, we measured the S-parameters of the microstrip lines and evaluated the propagation constant γ by applying mTRL calibration. Subsequently, we performed a 2-D full-wave EM simulation of the microstrip line using Ansys HFSS while enabling the causal Huray roughness model (the simulation setup is the same as in Fig. 3). In EM simulation, we set $\tan\delta = 0$. Then, optimization was performed according to the objective function in (30) up to 8 GHz. By this process, we obtained a sphere (snowball) radius of 0.4 μm with 50 spheres covering a flat area of 100 μm^2 as the parameters for the causal Huray roughness model. The measured and simulated data are summarized in Fig. 9.

For the second step, we compute $\epsilon_{r,\text{eff}}'$ and $\tan\delta_{\text{eff}}$ based on (23) and (24), where $R/(\omega L)$ is known from EM simulation. The results for $\epsilon_{r,\text{eff}}'$ and $\tan\delta_{\text{eff}}$ are shown in Fig. 10.

In the final step, we map both $\epsilon_{r,\text{eff}}'$ and $\tan\delta_{\text{eff}}$ to ϵ_r' and $\tan\delta$, respectively, using a second-order polynomial approximation as discussed in Section IV. The results for the frequency-dependent ϵ_r' and $\tan\delta$ are depicted in Fig. 11. In addition, we summarized our result at two frequencies in Table I. We can see a strong agreement between our results and the split cavity resonator data. However, we can recognize a slight discrepancy in $\tan\delta$ between the cavity measurements and our estimate, which is likely due to the metallization process which is not accounted for in the cavity measurements. In addition, it is clear to see that at low frequencies $\tan\delta$ is negative. This behavior is an artifact caused by the assumption that $\tan\delta$ is zero at these frequencies when performing the optimization problem to find the parameters of the roughness

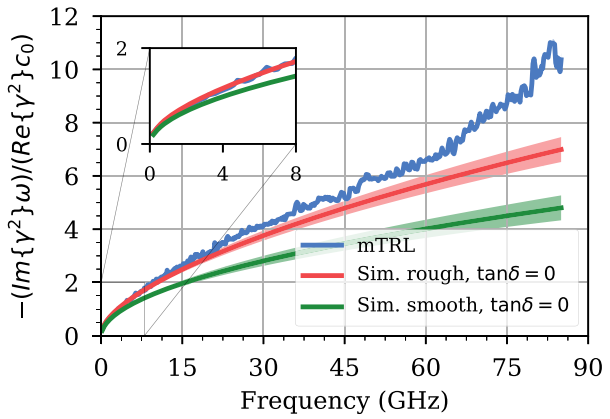

Fig. 9. Fitting EM simulations to the measurements at lower frequencies to obtain optimal parameters for the causal Huray roughness model.

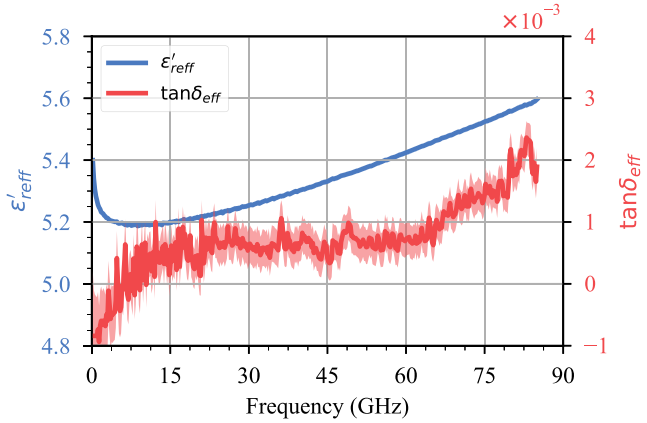

Fig. 10. Estimated effective dielectric constant $\epsilon'_{r,eff}$ and effective loss tangent $\tan\delta_{eff}$.

TABLE I

COMPARISON OF THE EXTRACTED DIELECTRIC PROPERTIES OF THE LTCC SUBSTRATE AT 60 GHz AND 79 GHz

	This Work		Cavity Measurements	
	ϵ'_r	$\tan\delta$	ϵ'_r	$\tan\delta$
60GHz	7.84± 0.094	0.00075± 0.00029	7.86	0.0012
79GHz	7.85± 0.086	0.00148± 0.00028	7.9	0.0015

model. Therefore, the negative values can be validly set to zero.

VI. DISCUSSION AND CONCLUSION

As alluded to in Section I, the methods to measure complex permittivity of dielectric substrates are hard to generalize at mm-wave frequencies. Moreover, some methods presented in the literature impose specific requirements, e.g., near-lossless dielectric behavior. The technique described in this article is no exception. However, the steps conducted in this work are carefully executed, and their validity is well-explained. For example, for estimating the impact of surface roughness,

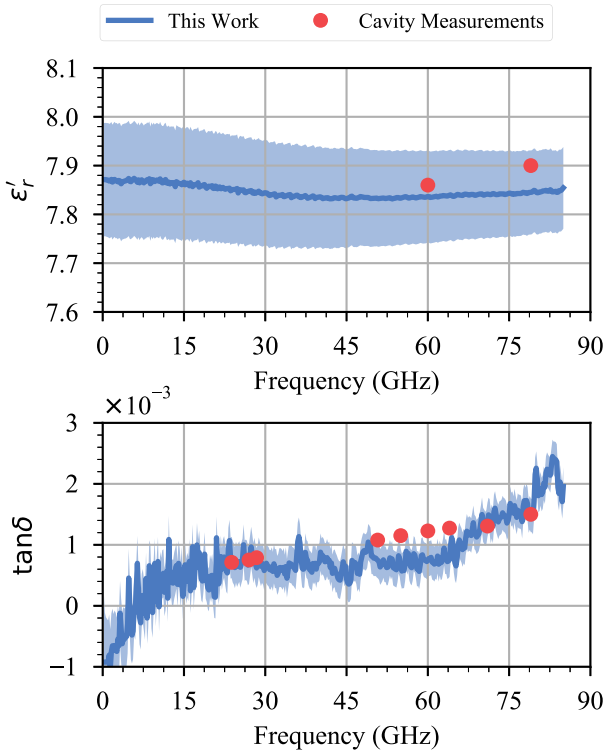

Fig. 11. Frequency-dependent estimation of ϵ'_r and $\tan\delta$ with their uncertainties, compared with split cavity resonator measurements.

we discussed that this should be achieved at low frequencies. At this regime, the skin depth is in the same range of roughness depth. In addition, at these frequencies, the dielectric loss is very low. However, this limitation already implies that estimating the losses due to roughness for lossy substrates at low frequencies is not practical. Fortunately, most dielectric substrates used in RF applications meet this criterion at low frequencies.

Another aspect we discussed is the validity of using EM simulations to obtain R and L while not fully knowing the complex permittivity of the dielectric. We highlighted that simulating R and L for the TEM propagation is fully valid even without knowing the permittivity of the dielectric substrate for nonmagnetic materials. We also showed that these quantities are individually not unique in non-TEM modes, e.g., quasi-TEM. However, the quantity $R/(\omega L)$ is unique and can be determined from EM simulation. In this way, we can estimate the effective dielectric constant and effective loss tangent.

In the last step, we introduced mapping functions to convert the effective quantities to the actual parameters of the substrate. We generalized these functions as polynomial functions of Nth order, where the coefficients are frequency-dependent to capture the dynamics of microstrip's quasi-TEM mode. In conclusion, the approach presented in this work provided consistent results for ϵ'_r and $\tan\delta$, which agreed well with split cavity resonator measurements.

ACKNOWLEDGMENT

The financial support by the Christian Doppler Research Association, the Austrian Federal Ministry for Digital and

Economic Affairs and the National Foundation for Research, Technology and Development is gratefully acknowledged. The authors would also like to thank the Electronic Based Systems Center (ebsCENTER) for their support with the measurement equipment.

REFERENCES

[1] *2.5.5.10 High Frequency Testing to Determine Permittivityand Loss Tangent of Embedded Passive Materials*, document IPC-TM-650 Test Methods Manual, IPC, Jul. 2005.

[2] *Standard Test Method for Relative Permittivity (Dielectric Constant) and Dissipation Factor of Polymer-Based Microwave Circuit Substrates*, document ASTM D3380-14, 2014.

[3] J. Coonrod, "Characterizing circuit materials at mmWave frequencies," *Microw. J.*, vol. 62, no. 5, p. 152, May 2019.

[4] J. Krupka, "Frequency domain complex permittivity measurements at microwave frequencies," *Meas. Sci. Technol.*, vol. 17, no. 6, pp. R55–R70, Apr. 2006, doi: 10.1088/0957-0233/17/6/r01.

[5] M. A. Stuchly and S. S. Stuchly, "Coaxial line reflection methods for measuring dielectric properties of biological substances at radio and microwave frequencies—A review," *IEEE Trans. Instrum. Meas.*, vol. IM-29, no. 3, pp. 176–183, Sep. 1980.

[6] Y. Kato and M. Horibe, "Broadband permittivity measurements up to 170-GHz using balanced-type circular-disk resonator excited by 0.8-mm coaxial line," *IEEE Trans. Instrum. Meas.*, vol. 68, no. 6, pp. 1796–1805, Jun. 2019.

[7] J. Baker-Jarvis, E. J. Vanzura, and W. A. Kissick, "Improved technique for determining complex permittivity with the transmission/reflection method," *IEEE Trans. Microw. Theory Techn.*, vol. 38, no. 8, pp. 1096–1103, Aug. 1990.

[8] K. E. Dudeck and L. J. Buckley, "Dielectric material measurement of thin samples at millimeter wavelengths," *IEEE Trans. Instrum. Meas.*, vol. 41, no. 5, pp. 723–725, Oct. 1992.

[9] A. Kazemipour *et al.*, "Design and calibration of a compact quasi-optical system for material characterization in millimeter/submillimeter wave domain," *IEEE Trans. Instrum. Meas.*, vol. 64, no. 6, pp. 1438–1445, Jun. 2015.

[10] Y. Wang, X. Shang, N. M. Ridler, T. Huang, and W. Wu, "Characterization of dielectric materials at WR-15 band (50–75 GHz) using VNA-based technique," *IEEE Trans. Instrum. Meas.*, vol. 69, no. 7, pp. 4930–4939, Jul. 2020.

[11] D. DeGroot, J. Jargon, and R. Marks, "Multiline TRL revealed," in *Proc. 60th ARFTG Conf. Dig., Fall*, Washington, DC, USA, Dec. 2002, pp. 131–155.

[12] R. B. Marks, "A multiline method of network analyzer calibration," *IEEE Trans. Microw. Theory Techn.*, vol. 39, no. 7, pp. 1205–1215, Jul. 1991.

[13] Y. Eo, W. R. Eisenstadt, and J. Shim, "S-parameter-measurement-based high-speed signal transient characterization of VLSI interconnects on SiOS-parameter-measurement-based high-speed signal transient characterization of VLSI interconnects on SiO_2-Si substrate 2-Si substrate," *IEEE Trans. Adv. Packag.*, vol. 23, no. 3, pp. 470–479, Aug. 2000.

[14] D. F. Williams, U. Arz, and H. Grabinski, "Characteristic-impedance measurement error on lossy substrates," *IEEE Microw. Wireless Compon. Lett.*, vol. 11, no. 7, pp. 299–301, Jul. 2001.

[15] N. B. Popovic *et al.*, "Materials characterization with multiple offset reflects at frequencies to 110 GHz," *IEEE Trans. Microw. Theory Techn.*, vol. 68, no. 1, pp. 184–195, Jan. 2020.

[16] R. B. Marks and D. F. Williams, "Characteristic impedance determination using propagation constant measurement," *IEEE Microw. Guided Wave Lett.*, vol. 1, no. 6, pp. 141–143, Jun. 1991.

[17] D. F. Williams and R. B. Marks, "Transmission line capacitance measurement," *IEEE Microw. Guided Wave Lett.*, vol. 1, no. 9, pp. 243–245, Sep. 1991.

[18] J. Zhang *et al.*, "Causal RLGC(f) models for transmission lines from measured S-parameters," *IEEE Trans. Electromagn. Compat.*, vol. 52, no. 1, pp. 189–198, Feb. 2010.

[19] P. G. Huray, O. Oluwafemi, J. Loyer, E. Bogatin, and X. Ye, "Impact of copper surface texture on loss: A model that works," *DesignCon*, vol. 1, pp. 462–483, Jun. 2010.

[20] E. Bracken, "A causal huray model for surface roughness," in *Proc. DesignCon*, vol. 4, p. 2880. [Online]. Available: https://www.researchgate.net/publication/256632915_A_Causal_Huray_Model_for_Surface_Roughness

[21] G. Gold and K. Helmreich, "A physical surface roughness model and its applications," *IEEE Trans. Microw. Theory Techn.*, vol. 65, no. 10, pp. 3720–3732, Oct. 2017.

[22] J. R. Brews, "Transmission line models for lossy waveguide interconnections in VLSI," *IEEE Trans. Electron Devices*, vol. ED-33, no. 9, pp. 1356–1365, Sep. 1986.

[23] R. B. Marks and D. F. Williams, "A general waveguide circuit theory," *J. Res. Nat. Inst. Standards Technol.*, vol. 97, no. 5, p. 533, Sep. 1992.

[24] J. R. Brews, "Characteristic impedance of microstrip lines," *IEEE Trans. Microw. Theory Techn.*, vol. MTT-35, no. 1, pp. 30–34, Jan. 1987.

[25] A. R. Djordjevic, R. M. Biljie, V. D. Likar-Smiljanic, and T. K. Sarkar, "Wideband frequency-domain characterization of FR-4 and time-domain causality," *IEEE Trans. Electromagn. Compat.*, vol. 43, no. 4, pp. 662–667, Nov. 2001.

[26] E. Hammerstad and O. Jensen, "Accurate models for microstrip computer-aided design," in *IEEE MTT-S Int. Microw. Symp. Dig.*, Washington, DC, USA, May 1980, pp. 407–409.

[27] E. Bogatin, D. Degroot, P. Huray, and Y. Shlepnev, "Which one is better? Comparing options to describe frequency dependent losses," *DesignCon*, vol. 1, pp. 469–494, 01 2013.

[28] M. Kirschning and R. Jansen, "Accurate model for effective dielectric constant of microstrip with validity up to millimetre-wave frequencies," *Electron. Lett.*, vol. 18, no. 6, pp. 272–273, Aug. 1982, doi: 10.1049/el_19820186.

[29] N. Hungerbühler, "An alternative quadratic formula," Tech. Rep., 2019. [Online]. Available: https://arxiv.org/abs/1702.05789

[30] M. Steer, *Microwave and RF Design: Transmission Lines*, vol. 2, 3rd ed. Raleigh, NC, USA: NC State Univ., 2019.

[31] *Evaluation of Measurement Data—Supplement 2 to the 'Guide to the Expression of Uncertainty in Measurement'—Extension to Any Number of Output Quantities*, Standard JCGM, 2011.

[32] B. D. Hall, "Evaluating the measurement uncertainty of complex quantities: A selective review," *Metrologia*, vol. 53, no. 1, pp. S25–S31, Dec. 2015, doi: 10.1088/0026-1394/53/1/s25.

Ziad Hatab (Student Member, IEEE) received the B.Sc. and Dipl.-Ing. (M.Sc.) degrees in electrical engineering from the Graz University of Technology, Graz, Austria, in 2018 and 2020, respectively, where he is currently pursuing the Ph.D. degree in information and communication engineering.

In 2020, he joined the Christian Doppler Laboratory TONI, Graz University of Technology, as a Research Member. His work focuses on millimeter-wave measurement techniques and calibration methods.

Michael Gadringer (Senior Member, IEEE) received the Dipl.-Ing. and Dr.techn. degrees from the Vienna University of Technology, Vienna, Austria, in 2002 and 2012, respectively.

He changed to the Institute of Microwave and Photonic Engineering, Graz University of Technology, Graz, Austria, in July 2010. Since 2016, he has been holding a tenure track research and teaching position with the Institute of Microwave and Photonic Engineering. In addition, he was a Visiting Researcher with Rohde&Schwarz GmbH, Munich, Germany, in 2017, and Infineon Technology AG, Neubiberg, Germany, in 2018. During his studies, he was involved in designing analog and digital linearization systems for power amplifiers and behavioral modeling of microwave circuits. He has authored or coauthored more than 20 journals articles and 52 conference papers. He holds four worldwide patents and has coedited the book *RF Power Amplifier Behavioral Modeling* (Cambridge University Press). In addition, he is involved in planning and implementing complex measurements, emphasizing calibration and deembedding techniques. His current research activities focus on developing and linearizing broadband microwave and millimeter-wave (mm-wave) communication systems.

Dr. Gadringer is a member of the IEEE P1765 standard working group on the recommended practice for estimating the Error Vector Magnitude of digitally modulated signals. In addition, he is contributing to the IEEE P2822 working group on the recommended practice for microwave, mm-wave, and terahertz on-wafer calibrations, deembedding, and measurements. The IEEE Instrumentation and Measurement Society selected him as a 2020 IEEE TRANSACTIONS ON INSTRUMENTATION AND MEASUREMENT (TIM) Outstanding Reviewer.

Mariam Habib received the bachelor's degree in electrical engineering from the Islamic University of Gaza (IUG), Gaza, Palestine, in 2014, and the master's degree in RF electronics from the ESIEE-Paris, Noisy-le-Grand, France, in 2018. She is currently pursuing the Ph.D. degree in millimeter-wave integrated circuits design with Infineon, Villach, Austria.

During her master's thesis, she was working on stability analysis of a 77-GHz PA with Infineon Technologies AG, Villach. She has gained experience in RFIC design, analysis, and testing methods and has worked with different simulation tools such as Cadence, ADS, and Silvaco TCAD Atlas. Since 2019, she has been employed as a University Assistant with the Graz University of Technology (TU-Graz), Graz, Austria, working on modeling and characterizing of the HF7 LTCC process, contributing her experience in simulation tools and measurement equipment.

Wolfgang Bösch (Fellow, IEEE) received the Dipl.Ing. degree from the Technical University of Vienna, Vienna, Austria, in 1985, the Ph.D. degree from the Graz University of Technology, Graz, Austria, in 1988, and the M.B.A. degree from the School of Management, University of Brad ford, Bradford, U.K., in 2004.

He has joined the Graz University of Technology to establish a new Institute for Microwave and Photonic Engineering. His Institute has more than 45 researchers, on average 60 publications per year and a research project turnover of €1.7 million per year. Previously, he was the Chief Technology Officer (CTO) of the Advanced Digital Institute, Shipley, U.K., a not-for-profit organization to promote research activities. Earlier he served as the Director of the Business and Technology Integration for RFMD, Reading, U.K. and for almost ten years he has been with Filtronic plc, Yeadon, U.K., as CTO of Filtronic Integrated Products and the Director of the Global Technology Group, New York, NY, USA. Before joining Filtronic, he has held positions with the European Space Agency (ESA), Paris, France, working on amplifier linearization techniques, with MPR-Teltech, Burnaby, BC, Canada, working on MMIC Technology Projects, and with the Corporate R&D Group of M/A-COM, Boston, MA, USA, where he worked on advanced topologies for high-efficiency power amplifiers. For four years he was with DaimlerChrysler Aerospace (now Airbus), Munich, Germany, working on T/R modules for airborne radar. He is currently the Dean of the Faculty of Electrical and Information Engineering, Graz University of Technology, which currently incorporates 13 Institutes and 18 Full Professors. He has published more than 150 articles and holds four patents.

Mr. Bösch is a fellow of the IET.